



## Adsorption of molybdenum(VI) by low-temperature biochar derived from activated sludge and application in reservoir water purification

Guoting Li<sup>a,b,\*</sup>, Shuaiyang Zhang<sup>a,b</sup>, Xiao Mi<sup>a,b</sup>, Yiping Guo<sup>a,b</sup>, Yujie Guo<sup>a,b</sup>, Tannaz Pak<sup>c</sup>

<sup>a</sup>School of Environmental and Municipal Engineering, North China University of Water Resources and Electric Power, Zhengzhou 450046, China, Tel. +86-371-69127436/+86-371-69127538; Fax: +86-371-65790239; emails: lipsonny@163.com (G.T. Li), handsomyang@126.com (S.Y. Zhang), mixiao@ncwu.edu.cn (X. Mi), guoyiping@ncwu.edu.cn (Y.P. Guo), guoyujie@ncwu.edu.cn (Y.J. Guo)

<sup>b</sup>Henan Key Laboratory of Water Environment Simulation and Treatment, North China University of Water Resources and Electric Power, Zhengzhou 450046, China

<sup>c</sup>School of Computing, Engineering, and Digital Technologies, Teesside University, Borough Road, Middlesbrough, TS1 3BX, UK, email: t.pak@tees.ac.uk

Received 19 September 2020; Accepted 26 March 2021

### ABSTRACT

At an industrial scale, significant quantities of solid activated sludge were produced as a by-product in wastewater treatment plants. In this contribution, activated sludge biochar was synthesized under oxygen-limited conditions with the purpose of adsorptive removal of Mo(VI) from contaminated water. Our experiments show that the sludge biochar have a better performance in Mo(VI) removal compared to the raw sludge. Additionally, we report that demineralized biochar (pyrolyzed at 200°C, D-BC200) performs better than sludge biochar samples pyrolyzed at other temperatures. From microscopic point of view, D-BC200 particles are shown to be smaller than 20 μm in size with a porous structure. The outcomes of surface analysis indicated that D-BC200 had abundant surface functional oxygen-containing groups. This facilitated the uptake of Mo(VI). We performed both non-linear and linear pseudo-second-order kinetics modelling to describe the experimental kinetics observed in our experiments. We conclude that both approaches are suitable for modelling the chemisorption process involved in removal of Mo(VI). Langmuir model better described adsorption isotherm, and the maximal adsorption capacity at 298 K was 82.1 mg/g, which was comparatively higher among the adsorbents reported. The enthalpy and entropy of the adsorption process are -39.3 kJ/mol and -125.6 J/mol K, respectively. This indicated that the adsorption process was spontaneous and endothermic. Both coexisting anions and natural organic matter could inhibit adsorption of Mo(VI) to some extent. When D-BC200 was applied for the removal of Mo(VI) from natural reservoir water, complete removal of Mo(VI) was observed.

*Keywords:* Sludge biochar; Mo(VI); Adsorption; Mechanism; Water purification

### 1. Introduction

Adsorption process is one of the most adaptable processes applied in advanced water and wastewater treatment applications. In adsorption process pollutants are transferred

from one phase to another phase. The process is known to benefit from high efficiency, ease of operation, and cost-effectiveness [1,2]. As such, a number of common adsorbents (e.g., activated carbon and bentonite) have been widely applied in industrial application. However, application of

\* Corresponding author.

commercial activated carbon is limited by its complicated production technologies and its relatively high cost of production. Therefore, from a practical point of view, low-cost adsorbents, both considering the production and application costs, are in high demand.

Recently, attention has been focused on production of low-cost, carbon-based adsorbents such as raw biomass and biomass-related biochar. Raw biomass is abundantly available globally. Mainly produced as agricultural by-products, raw biomass is a low-cost alternative adsorbent with reasonable effectiveness. It has been shown that wide variety of organic contaminants and heavy metals can be efficiently removed from water by low-cost biomass adsorbents [1,3,4]. The key disadvantage of using raw biomass as an adsorbent is the possibility of organic leaching and hence introduction of a secondary pollution source.

Biochar derived from a versatile source of biomass has shown to offer a solution to this problem. Biochar displays an effective adsorption property when applied in water and wastewater treatment. Biochar is a pyrogenic-charcoal material derived from thermochemical conversion (pyrolysis) of carbon-rich biomass in an oxygen-limited environment [5,6]. The pyrogenic biochar is significantly more stable compared to the raw biomass. It is worth noting that the abundance of oxygen-containing groups (C=O, C-OH, COOH) in biochar improves its capacity for sorption of contaminants from aqueous phase [7,8]. Hence, biochar is recognized as a relatively low-cost adsorbent for removal of environmental contaminants.

Molybdenum is an essential micronutrient for enzymes. It contributes to the effective function of enzymes in biological and physiological processes in humans and animals [9]. The World Health Organization recommends that molybdenum concentration in drinking water should not exceed 70  $\mu\text{g/L}$ . However, molybdenum levels are found to be in the order of milligrams per liter in some aquatic systems [9]. Molybdenum is widely used in the manufacturing of semiconductors and in the optoelectronic industry. The discharged effluent streams of these industries are in need of better treatment. As a trace element, molybdenum is not removed completely from drinking water via traditional purification processes. In recent years, adsorption process has become one of the most popular techniques for removing trace elements from aqueous solutions [10,11]. Brion-Roby et al. [12] found that the maximum adsorption capacity that a chitosan sorbent achieved was 123 mg/g for the removal of molybdate ions. The virgin and calcined wheat bran is also used for molybdenum removal. For this, the uptake of molybdenum increased with increasing temperature, and the maximum adsorption capacity of WB1000 was found to be 84.0 mg/g [10]. Besides, multiwalled carbon nanotubes modified by NaClO solution display high adsorption capacity and less attrition of molybdenum through 10 cycles of adsorption and desorption [13].

In this research, activated sludge from a local wastewater treatment plant was used as biomass resource to prepare sludge biochar under oxygen-limited conditions. Trace element molybdenum was efficiently adsorbed by the prepared sludge biochar. The effect of pyrolytic temperature, biochar dose and solution pH was investigated. Adsorption kinetics and thermodynamics were also discussed. A practical

source water containing molybdenum was subjected for adsorption further to check the adsorption capability of sludge biochar.

## 2. Materials and methods

### 2.1. Materials

Analytical grade ammonium heptamolybdate ( $(\text{NH}_4)_6\text{Mo}_7\text{O}_{24}\cdot 4\text{H}_2\text{O}$ , Macklin Reagent Ltd., Shanghai, China) was employed to prepare a stock solution of Mo(VI). The other chemicals used were of analytical grade. Deionized (DI) water was used to prepare solutions throughout the study. The natural source water samples containing Mo(VI) were collected from watershed of Luhun Reservoir (Luoyang City, China).

### 2.2. Preparation of sludge biochar

The municipal activated sludge was collected from the dewatering stage of Matougang Wastewater Treatment Plant (Zhengzhou City, China). The collected sludge was air-dried, ground and screened through a 40 mesh sieve for further use. The detailed preparation of sludge biochar can be referred to our previous study [14]. The activated sludge was pyrolyzed in a muffle furnace at selected temperatures (200°C, 300°C, 400°C, 500°C and 600°C) for 2 h. These biochars were also treated in a 4 mol/L HCl acid solution to get demineralized biochars for subsequent use. These demineralized sludge biochars were hereafter referred to as D-BC200, D-BC300, D-BC400, D-BC500 and D-BC600, respectively wherein the suffix number represented the pyrolytic temperature.

### 2.3. Characterization

The surface morphology of the raw sludge and related biochars pyrolyzed at different temperatures was characterized using a Philips Quanta-2000 (Netherlands) scanning electron microscope (SEM) coupled with an energy-dispersive X-ray (EDX) spectrometer. Chemical analysis was performed using X-ray photoelectron spectroscopy (ESCALAB 250Xi, XPS, USA) technique. The acidic functional groups (i.e., carboxyl, lactonic, and phenolic) was determined using Boehm's titration method [15,16]. Zeta potential of D-BC200 was measured on the Zetasizer Nano S system (Malvern, UK).

### 2.4. Batch adsorption studies

Adsorption of molybdenum (Mo(VI)) onto the sludge biochars were performed in batch experiments. The stock solutions of Mo(VI) (500 mg/L) were prepared by dissolving ammonium heptamolybdate in DI water. All working solutions with the desired concentration were prepared by diluting the stock solution with DI water. Sludge biochar (10.0 mg) was added to conical flasks containing 50 mL solution with a Mo(VI) concentration of 5 mg/L. Constant and vigorous stirring was maintained by mechanical agitation for 24 h. For the kinetics study, 200 mg of sludge biochar were added to 1,000 mL solution with initial Mo(VI) concentration of 20 mg/L. The adsorption

reaction was carried out at 298 K except where the effect of reaction temperature was under study. All solution pH values were maintained at neutral pH except the study of pH effect. Solution pH adjustment was conducted by the addition of dilute HCl or NaOH solutions.

### 2.5. Analysis methods

After adsorption, samples were collected and filtered through a 0.45  $\mu\text{m}$  syringe membrane before analysis. Shimadzu UV-Visible (Japan) recording UVmini-1240 spectrophotometer was used for measuring the concentration of Mo(VI) by colorimetric method and the wavelength of maximum absorption at 465 nm was fixed for monitoring [17].

The removal percentage of Mo(VI) was given by:

$$R = \left(1 - \frac{C_t}{C_0}\right) \times 100\% \quad (1)$$

The adsorption capacities ( $q_e$ ,  $q_t$ ) were calculated as follows:

$$q_e = \frac{(C_0 - C_e)V}{W} \quad (2)$$

$$q_t = \frac{(C_0 - C_t)V}{W} \quad (3)$$

where  $q_e$  and  $q_t$  (mg/g) are the adsorption capacities at equilibrium and a time  $t$  (min);  $C_0$ ,  $C_e$  and  $C_t$  (mg/L) are the concentrations of Mo(VI) at initial stage, equilibrium and a time  $t$  (min), respectively;  $V$  (L) is the volume of solution, and  $W$  (g) is the mass of the sludge biochar used.

## 3. Results and discussion

### 3.1. Effect of pyrolytic temperature of sludge biochar and biochar dose on Mo(VI) uptake

As for Mo speciation, the oxidation state of this metal can change from  $-2$  to  $+6$  depending on the solution pH and electric potential, while Mo occurs principally in the hexavalent oxidation state as molybdate oxoanions ( $\text{MoO}_4^{2-}$ ) [18]. By contrast, as the contents of C, H and O on sludge biochar varied with the pyrolytic temperature, the surface properties of biochars including the contents of surface functional groups were expected significantly altered accordingly. Hence, the effect of pyrolytic temperature of sludge biochar on Mo(VI) uptake was investigated, as illustrated in Fig. 1a. Typically, the Mo(VI) uptakes on the raw sludge, D-BC200, BC300 and BC600, at 24 h, were 1.05, 4.70, 2.20 and 2.75 mg/g, respectively. Apparently, the sludge biochar had a better performance in Mo(VI) removal compared to the raw sludge, while D-BC200 displayed better adsorption capacity compared to other sludge biochars involved. This indicated that the specific surface chemistry of D-BC200 was quite beneficial for Mo(VI) uptake. Meanwhile, the low pyrolytic temperature for biochar preparation can save a lot of energy, while the yield percentage of D-BC200 (about 90%) is much higher than

other biochars. Low-temperature production is advantageous for biochar utilization. As such, the D-BC200 was selected for the following tests from a practical point of view. Concurrently, the effect of sludge biochar D-BC200 dose on Mo(VI) uptake was also explored and presented in Fig. 1b. The Mo(VI) uptakes at D-BC200 dose of 10, 20 and 40 mg reached 4.70, 2.80 and 1.51 mg/g, respectively. An increased dose of D-BC200 could significantly improve the removal of Mo(VI).

### 3.2. Effect of solution pH on Mo(VI) adsorption kinetics

The effect of solution pH on the adsorption kinetics of Mo(VI) by the sludge biochar D-BC200 was investigated at pH 5, 7 and 9, respectively. Typical kinetics models, including the Elovich model, the pseudo-first-order and pseudo-second-order models were used to fit the experimental data.

The non-linear and linear pseudo-first-order models are expressed as [19]:

$$q_t = q_e (1 - e^{-k_1 t}) \quad (4)$$

$$\ln(q_e - q_t) = \ln q_e - k_1 t \quad (5)$$

The non-linear and linear pseudo-second-order models can be expressed as [20]:

$$q_t = \frac{k_2 q_e^2 t}{1 + k_2 q_e t} \quad (6)$$

$$\frac{t}{q_t} = \frac{1}{k_2 q_e^2} + \frac{t}{q_e} \quad (7)$$

where  $q_e$  and  $q_t$  are the adsorption capacities (mg/g) of the sludge biochar D-BC200 at equilibrium and at time  $t$  (min), respectively;  $k_1$  ( $\text{min}^{-1}$ ) and  $k_2$  ( $\text{g}/(\text{mg min})$ ) are the adsorption rate constant for the pseudo-first-order and pseudo-second-order model, respectively.

The Elovich model, which is used to describe chemisorption occurring on a solid-liquid interface, can be expressed as [21,22]:

$$q_t = k \ln(t) + a \quad (8)$$

where  $a$  (g mg/min) and  $k$  (mg/g) are constants.

For simplicity, the non-linear simulation at pH 5, 7 and 9 is plotted in Fig. 2. It can be observed that 88.9% of Mo(VI) were adsorbed on D-BC200 within the initial 120 min, followed by a slower adsorption phase. The adsorption equilibrium can be achieved within 24 h. From Fig. 2, although the three kinetic models could fit the experimental data, only pseudo-second-order model was the best to simulate the data as the experimental points were much close to the fitted curve of pseudo-second-order model. Further, from the simulated kinetic parameters listed in Table 1, the determined coefficients ( $R^2$ ) values of the non-linear pseudo-second-order kinetics model were all much higher than those of the non-linear pseudo-first-order and Elovich model. The calculated  $q_e$  values were much

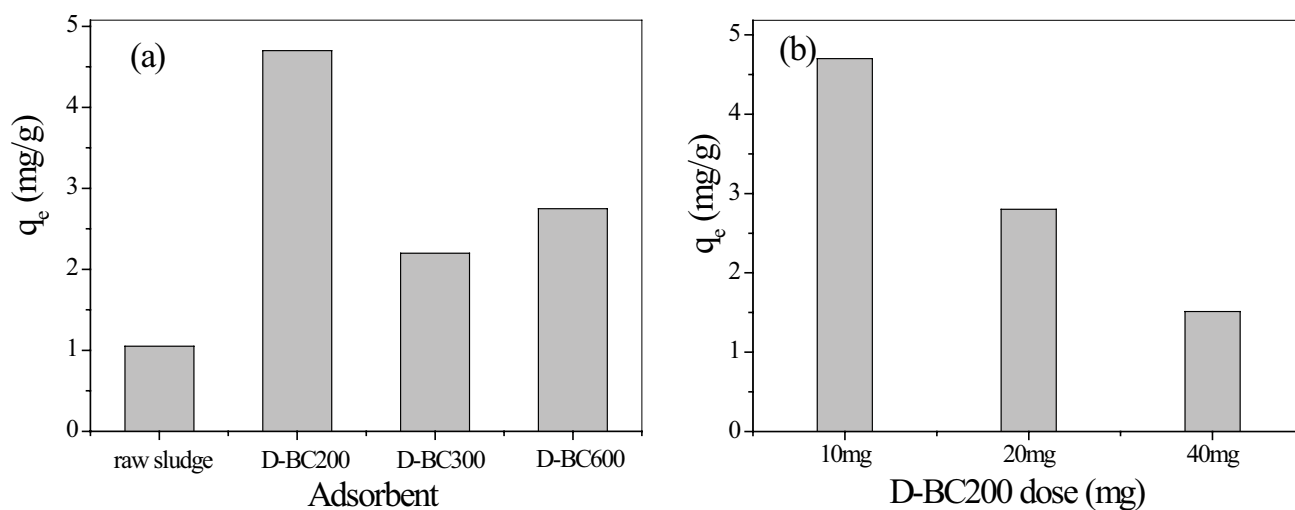


Fig. 1. Effect of pyrolytic temperature of sludge biochar (a) and biochar D-BC200 dose (b) on Mo(VI) uptake.

close to the experimental values using the pseudo-second-order kinetics model as well. Further, from Figs. 2d and e, linear pseudo-first-order kinetics model failed to describe the adsorption kinetics while linear pseudo-second-order kinetics model was a better choice as the data points were much close to its simulated curves. The higher  $R^2$  values of the linear pseudo-second-order kinetics model listed in Table 2 confirmed the result as well. Apparently, the pseudo-second-order kinetics model fitted the experimental data better, and it can be deduced that Mo(VI) uptake on D-BC200 was controlled by a chemisorption process.

On the other hand, from Fig. 2 and Table 1, the adsorption process was highly pH-dependent, and the uptake of Mo(VI) increased with decreasing solution pH. As the biochars are normally negatively charged [6], D-BC200 surface with abundant oxygen-containing functional groups could become more negatively charged with an increase in solution pH. Meanwhile, the distribution of different Mo(VI) species found in solutions are  $\text{MoO}_4^{2-}$ ,  $\text{HMoO}_4^-$ ,  $\text{H}_2\text{MoO}_4$ ,  $\text{Mo}_7\text{O}_{21}(\text{OH})_3^{3-}$ ,  $\text{Mo}_7\text{O}_{21}(\text{OH})_2^{4-}$ ,  $\text{Mo}_7\text{O}_{23}(\text{OH})_5^-$ , and  $\text{Mo}_7\text{O}_{24}^{6-}$  [23]. The predominant charges of Mo(VI) are negative. As such, it is expected that the electrostatic attractive force could be enhanced with decreasing solution pH. As illustrated in Table 1, at pH 5, 7 and 9, the simulated  $q_e$  values from non-linear pseudo-second-order kinetics model are 5.37, 3.61 and 1.28 mg/g, respectively. This indicated that electrostatic force and hydrogen bond played a major role during adsorption. At the same time, it demonstrated that the pH-sensitive functional groups such as carboxyl and phenolic groups contributed to Mo(VI) removal to a large extent.

### 3.3. Adsorption isotherm

Adsorption isotherm study for Mo(VI) onto D-BC200 was conducted at three different reaction temperatures including 288, 298 and 308 K. Traditional isothermal models including Langmuir and Freundlich equations were used to fit the experimental data.

The Langmuir equation is represented as [24]:

$$q_e = \frac{q_m k_L C_e}{1 + k_L C_e} \quad (9)$$

The Freundlich equation is represented as [25]:

$$q_e = k_F C_e^{1/n} \quad (10)$$

where  $q_e$  is the amount of Mo(VI) adsorbed onto D-BC200 (mg/g),  $C_e$  is the equilibrium concentration (mg/L),  $q_m$  is the maximum adsorption capacity of D-BC200 (mg/g),  $k_L$  is the equilibrium adsorption constant related to the affinity of binding site (L/mg),  $k_F$  ( $\text{mg}^{(1-1/n)} \text{L}^{1/n}/\text{g}$ ) is the Freundlich constants related to the adsorption capacity.

As illustrated in Fig. 3, D-BC200 had a strong adsorption capability for Mo(VI) at the three temperatures, while the Mo(VI) uptake increased with decreasing reaction temperature, indicating an endothermic adsorption process. The adsorption isotherm data at the three temperatures were simulated by Langmuir and Freundlich models. The experimental points were quite close to the simulated curves from Langmuir and Freundlich models. Actually, both isotherm models well described the adsorption process under the three temperatures. From the simulated isotherm parameters listed in Table 3, the  $R^2$  values from Langmuir models were slightly higher than those from Freundlich models, indicating that the adsorption was dominated by single-layer adsorption. At the same time, the results of fitting by the Langmuir equation showed that the maximal adsorption capacities at 288, 298 and 308 K were 101.9, 82.1 and 74.3 mg/g, respectively. This indicates that the decreased temperature favored the Mo(VI) uptake and the adsorption process was endothermic in nature. Additionally, from Table 4, D-BC200 has a comparatively higher adsorption capability for Mo(VI) uptake among various adsorbents.

### 3.4. Adsorption thermodynamics

Thermodynamic parameters associated with the adsorption process including standard free energy change ( $\Delta G^\circ$ ),

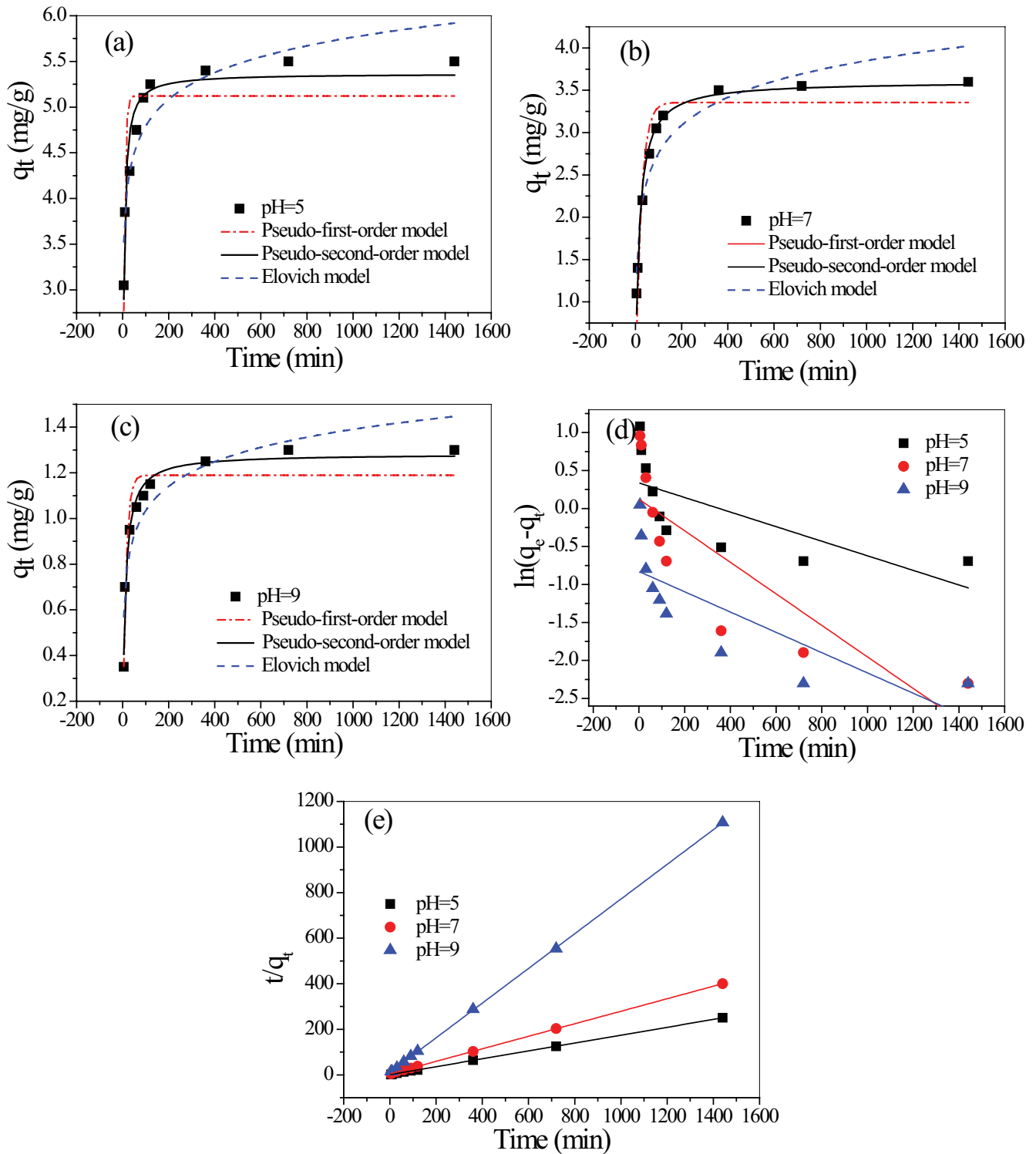


Fig. 2. Non-linear simulation at pH 5 (a), 7 (b), 9 (c), linear pseudo-first-order (d) and linear pseudo-second-order (e) simulation for the adsorption of Mo(VI) onto D-BC200.

standard enthalpy change ( $\Delta H^\circ$ ) and standard entropy change ( $\Delta S^\circ$ ) were calculated using the following equations:

$$\Delta G^\circ = -RT \ln k_0 \tag{11}$$

$$\Delta G^\circ = \Delta H^\circ - T\Delta S^\circ \tag{12}$$

$$\ln k_0 = -\frac{\Delta H^\circ}{RT} + \frac{\Delta S^\circ}{R} \tag{13}$$

In these equations,  $T$  is in Kelvin;  $\Delta H^\circ$  is the entropy of adsorption and  $R$  is the universal gas constant (8.314 J/mol K). The thermodynamic equilibrium constant  $k_0$  for the adsorption process was determined by plotting  $\ln q_e/C_e$  vs.  $q_e$  and extrapolating to zero  $q_e$  using a graphical method [33]. The values of  $\Delta H^\circ$  and  $\Delta S^\circ$  can be obtained from the slope and intercept of a plot  $\ln k_0$  vs. the reciprocal of absolute temperature ( $1/T$ ) (Fig. 4).

It can be seen from Table 5 that the enthalpy and entropy of the adsorption process are  $-39.3$  kJ/mol and  $-125.6$  J/mol K, respectively. The negative value of  $\Delta G^\circ$  and positive value of  $\Delta H^\circ$  indicated that the adsorption process is spontaneous and endothermic, which is consistent with the afore-mentioned results.

### 3.5. Adsorption mechanism

The SEM image and zeta potential of the biochar D-BC200 are shown in Fig. 5. The morphologies of the biochar D-BC200 clearly demonstrate a quite irregular structure. Most of the biochar D-BC200 particles are below  $20 \mu\text{m}$  in size, and a porous structure is apparently observed within the particles. From EDX analysis, the carbon contents of the raw sludge and D-BC200 are 50.8% and 53.0%, respectively, while the oxygen content decreased from 37.8% of the raw sludge to 24.9% of the D-BC200. From Fig. 5b, the zeta potential of the biochar D-BC200 was around  $-10$  mV, indicating that D-BC200 is mainly negatively charged on its surface. By Boehm titration, the contents of acidic functional groups including carboxyl, lactonic and phenolic

groups on D-BC200 were detected to be as much as 0.758, 0.132 and 0.160 mmol/g, respectively. As stated above, these acidic functional groups might have been responsible for the excellent adsorption performance for Mo(VI).

As the states of carbon and oxygen elements are quite complicated on biochar surface, XPS spectra of O1s, C1s and wide scan XPS spectra of the biochar D-BC200 were measured and presented in Fig. 6. For full XPS scan illustrated in Fig. 6a, an obvious difference is that a photoelectron peak at around 399.7 eV of N1s was observed on D-BC200, indicating a comparatively higher N content on D-BC200 than that on BC600.

From Figs. 6b and c, the O1s intensity of D-BC200 was apparently higher than that of D-BC600, while the C1s intensity of D-BC600 was much higher than that of D-BC200. These demonstrated a higher O content on D-BC200 and higher C content on D-BC600, which is consistent with the afore-mentioned results. Further, the asymmetric C1s XPS patterns for the two biochars can be quantitatively differentiated into five different carbon stages as illustrated in Figs. 6d and e, including the  $\text{sp}^2$  hybridized carbon (C=C, 284.6 eV), the  $\text{sp}^3$  hybridized carbon (C-C, about 285.0 eV), alcohol/ether group (C-O, about 286.2 eV), and carbonyl group (C=O, about 287.4 eV) and carboxyl acid/ester group (O-C=O, about 288.7 eV) [34,35]. From Figs. 6d and e, it demonstrated that both biochars have abundant C-O and O-C=O groups on their surface, while the abundance of C-O and O-C=O groups on D-BC200 is much higher than that on D-BC600 judged from the intensities of peaks. Although D-BC600 had a very strong photoelectron peak at around 287.4 eV of carbonyl groups, the carbonyl groups did not contribute to the adsorption considering the adsorption capability of D-BC600. Besides, from Table 6, the chemical state assignments demonstrated that the contents of C-O and O-C=O groups are much higher on D-BC600 than those

Table 1  
Non-linear kinetics parameters simulated by the pseudo-first-order, pseudo-second-order and Elovich models for Mo(VI) adsorption on D-BC200

Model	Parameters	pH=5	pH=7	pH=9
Pseudo-first-order	$q_e$ (mg/g)	5.12	3.36	1.19
	$k_1$ ( $\text{min}^{-1}$ )	0.156	0.041	0.071
Pseudo-second-order	$R^2$	0.758	0.900	0.897
	$q_e$ (mg/g)	5.37	3.61	1.28
	$k_2$ (g/(mg min))	0.044	0.017	0.072
Elovich	$R^2$	0.937	0.985	0.976
	$a$	2.85	0.579	0.322
	$k$	0.422	0.473	0.155
	$R^2$	0.858	0.896	0.846

Table 3  
Langmuir and Freundlich isotherm parameters for the adsorption of Mo(VI) onto D-BC200

Model	Parameters	288 K	298 K	308 K
Langmuir	$q_{\text{max}}$ (mg/g)	101.9	82.1	74.3
	$k_L$ (L/mg)	0.033	0.022	0.020
	$R^2$	0.992	0.995	0.983
Freundlich	$k_f$ ( $\text{mg}^{(1-1/n)} \text{L}^{1/n}/\text{g}$ )	10.7	5.94	4.80
	$n$	2.36	2.09	2.02
	$R^2$	0.916	0.940	0.915

Table 2  
Linear kinetics parameters simulated by the pseudo-first-order and pseudo-second-order models for Mo(VI) adsorption on D-BC200

	Pseudo-first-order model			Pseudo-second-order model		
	$q_e$ (mg/g)	$k_1$ ( $\text{min}^{-1}$ )	$R^2$	$q_e$ (mg/g)	$k_2$ (mg/g min)	$R^2$
pH=5	1.40	0.001	0.432	5.79	0.020	0.999
pH=7	1.13	0.002	0.660	3.64	0.017	0.999
pH=9	0.44	0.001	0.560	1.31	0.055	0.999

Table 4  
Comparison of Mo(VI) adsorption capacities on various sorbents

Sorbents	$q_m$ (mg/g)	Solution pH	References
Sludge biochar D-BC200	82.1	7	This study
WB200	33.4	N.A.	[10]
WB1000	84.0	N.A.	[10]
Maghemite	33.4	5	[26]
Nano-magnetic $\text{CuFe}_2\text{O}_4$	30.6	2.8	[9]
Mesoporous zirconium silicate	22.8	N.A.	[27]
NaOCl-oxidized multiwalled carbon nanotubes	20.2	Neutral	[13]
$\text{ZnCl}_2$ activated coir pith carbon	14.4	N.A.	[28]
Waste Fe(III)/Cr(III) hydroxide	12.3	Initial pH 4.0	[29]
Iron-based adsorbents	10.4	3 mol/L $\text{HNO}_3$	[30]
Chitosan adsorbent	124.3	7.8	[12]
Mo(VI) ion-imprinted polymer	126.1	3	[31]
Microcrystalline anthracene modified with 8-hydroxyquinoline	45.1	N.A.	[32]

N.A. = Not available;

The suffix of BC indicates the pyrolytic temperature for biochar.

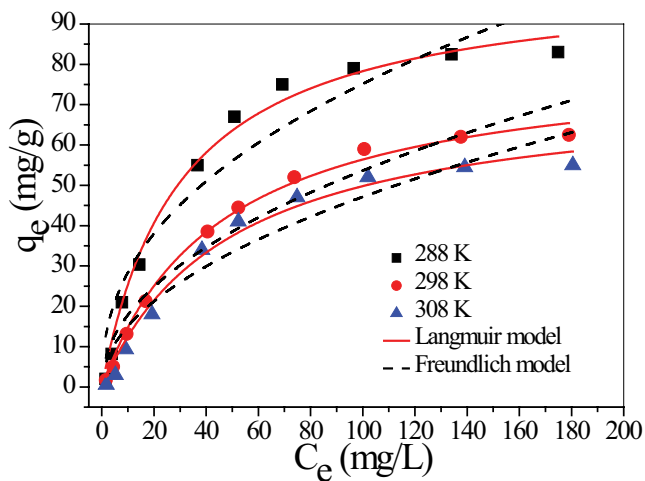


Fig. 3. Langmuir and Freundlich isotherms for the adsorption of Mo(VI) onto D-BC200 at 288, 298 and 308 K.

on D-BC200. However, the total amount of C–O and O–C=O groups on D-BC600 is still particularly lower than that on D-BC200. As such, the surface functional oxygen-containing groups still played the most important roles for Mo(VI) removal.

The existing Mo(VI) species are significantly affected by solution pH. The concentrations of poly-molybdenum acid ions including  $\text{HMo}_7\text{O}_{24}^{5-}$  and  $\text{H}_2\text{Mo}_7\text{O}_{24}^{4-}$  increase dramatically, while the concentrations of  $\text{H}_2\text{MoO}_4$  and  $\text{HMoO}_4^-$  become insignificant especially when Mo(VI) species is higher than 1 mg/L [17]. The concentration of Mo(VI) in this research was 5 mg/L and  $\text{HMo}_7\text{O}_{24}^{5-}$  and therefore  $\text{H}_2\text{Mo}_7\text{O}_{24}^{4-}$  were deduced to be the main Mo(VI) species accordingly. On the other hand, it was confirmed that Mo(VI) adsorption onto adsorbents is dependent on the surface chemical nature rather than the porosity characteristics [13]. The surface total acidic sites of carbonaceous adsorbents

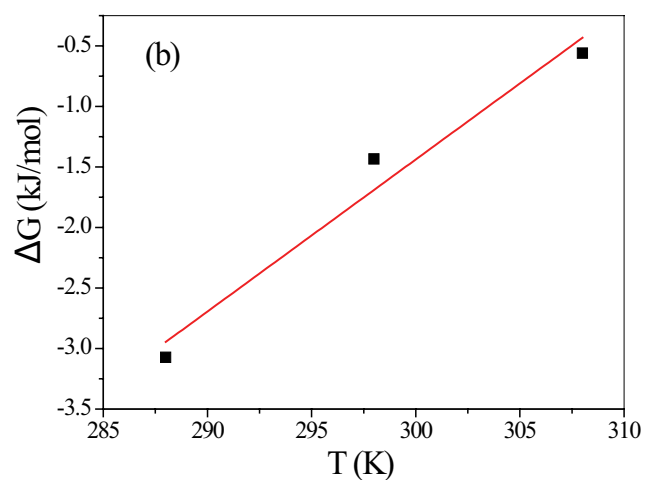
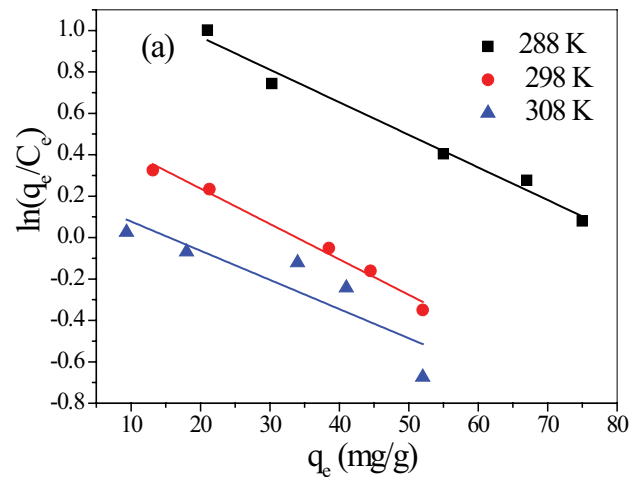


Fig. 4. Plots of  $\ln q_e/C_e$  vs.  $q_e$  for Mo(VI) adsorption on D-BC200 (a) and changes of free energy (thermodynamic calculations) (b).

Table 5  
Thermodynamic parameters at different reaction temperatures

T (K)	$\ln k_0$	$\Delta G^\circ$ (kJ/mol)	$\Delta H^\circ$ (kJ/mol)	$\Delta S^\circ$ (J/mol K)
288	1.28	-3.07	-39.3	-125.6
298	0.58	-1.44	-39.3	-125.6
308	0.22	-0.56	-39.3	-125.6

Table 6  
Chemical state assignments for D-BC200 and D-BC600 (%)

	C=C	C-C	C-O	C=O	CO-O
D-BC200	34.3	58.3	3.85	/	3.54
D-BC600	27.0	26.2	17.7	14.5	14.6

had a direct correlation with heavy metal ion adsorption from aqueous solutions [36]. Ogata et al. [10] reported that the hydroxyl groups (-OH) present on the surface of wheat bran act as the major functional groups in Mo(VI) adsorption. As such, the surface acidic functional groups have actually contributed to the adsorption of Mo(VI) onto D-BC200 dramatically. In terms of carbonaceous adsorbents, both the content and the species of surface acidic functional groups should be considered for removal of heavy metal ions.

### 3.6. Effect of co-existing anions and natural organic matter on Mo(VI) adsorption

As coexisting anions and natural organic matter (NOM) are ubiquitous in environmental waters, the effect of coexisting anions and NOM (humic acid) were investigated and illustrated in Fig. 7. Naturally occurring anions such as  $\text{HCO}_3^-$ ,  $\text{Cl}^-$ ,  $\text{SO}_4^{2-}$  and  $\text{HPO}_4^{2-}$  are negatively charged, which could compete with these negatively-charged Mo(VI) species for the uptake on D-BC200. From Fig. 7a, the four anions were evidently capable of inhibiting the Mo(VI) uptake, in which  $\text{HPO}_4^{2-}$  had the strongest inhibiting effect. Meanwhile, from Fig. 7b, the uptake of Mo(VI) declined moderately with increasing NOM dosage. This indicated that the inhibiting effect of NOM on the removal of Mo(VI) from natural waters could be insignificant to some extent.

### 3.7. Application for environmental reservoir water treatment

In order to check the practical applicability of the biochar D-BC200 for Mo(VI) removal, natural water samples containing Mo(VI) were collected from watershed of Luhun Reservoir (Luoyang City, China) during spring. The Mo(VI) concentrations in spring samples were 0.164 mg/L, respectively. The pH of reservoir water was around 8 and  $\text{COD}_{\text{Mn}}$  was about 4.0. By adding 10 mg of D-BC200 in 50 mL of reservoir water, the Mo(VI) concentration became undetected after 24 h of shaking. As such, biochar D-BC200 has the potential for water purification in practical water plant.

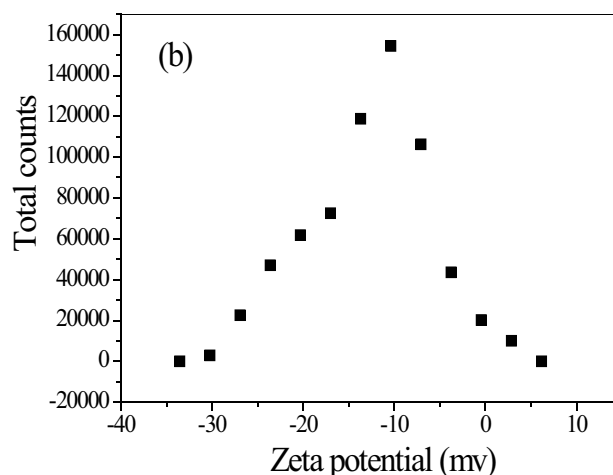
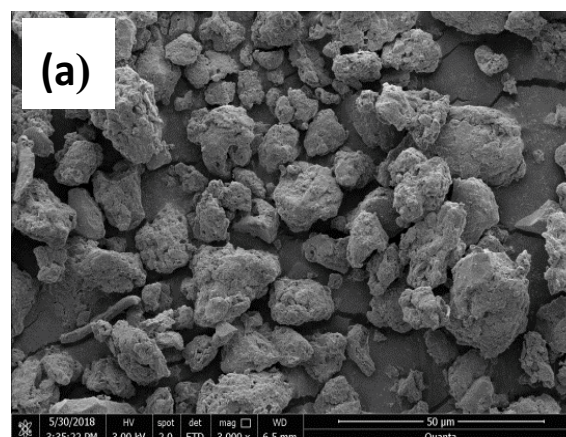


Fig. 5. SEM image (a) and zeta potential (b) of the biochar D-BC200.

## 4. Conclusions

Pyrogenic sludge biochar derived from an industrial waste, activated sludge, was synthesized and utilized for adsorptive removal of Mo(VI) from contaminated water. The sludge biochar performed better than the raw sludge, while D-BC200 displayed better adsorption capacity compared to other sludge biochars. Both the non-linear and linear pseudo-second-order kinetics model better described the experimental kinetics as compared to the Elovich and linear pseudo-first-order model, indicating a chemisorption process. Langmuir isotherm model described adsorption isotherm slightly better than Freundlich model. The maximal adsorption capacity at 298 K was as much as 82.1 mg/g. This indicated that the adsorption process was spontaneous and endothermic. The surface functional oxygen-containing groups played the most important role for Mo(VI) removal. Both coexisting anions and natural organic matter could inhibit adsorption of Mo(VI) to some extent. Mo(VI) was completely removed when D-BC200 was applied for the removal of Mo(VI) from natural reservoir water.

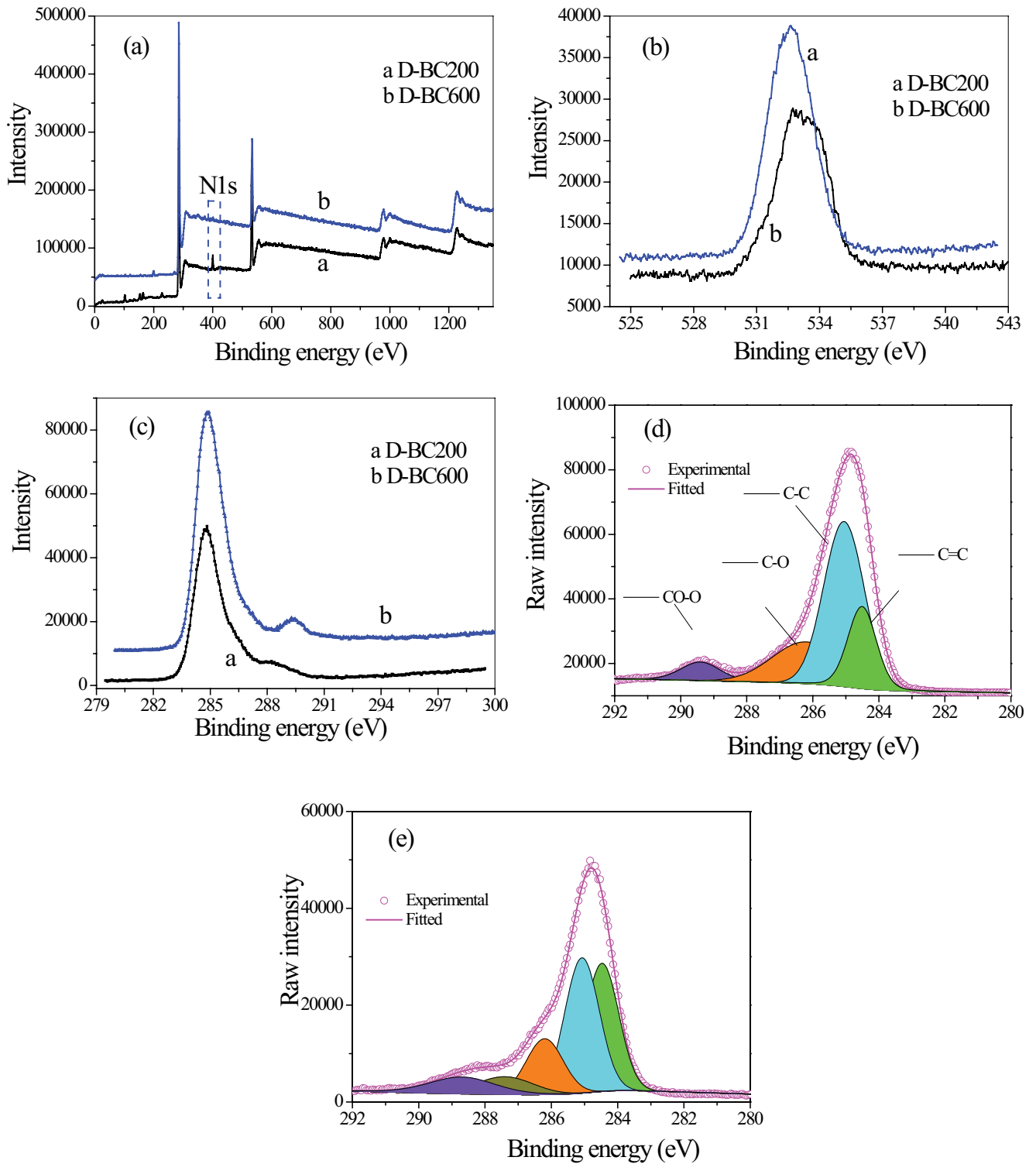


Fig. 6. XPS full scans spectra (a), O1s (b), wide scan C1s (c) of the D-BC200 and D-BC600, C1s of D-BC200 (d) and C1s of D-BC600 (e).

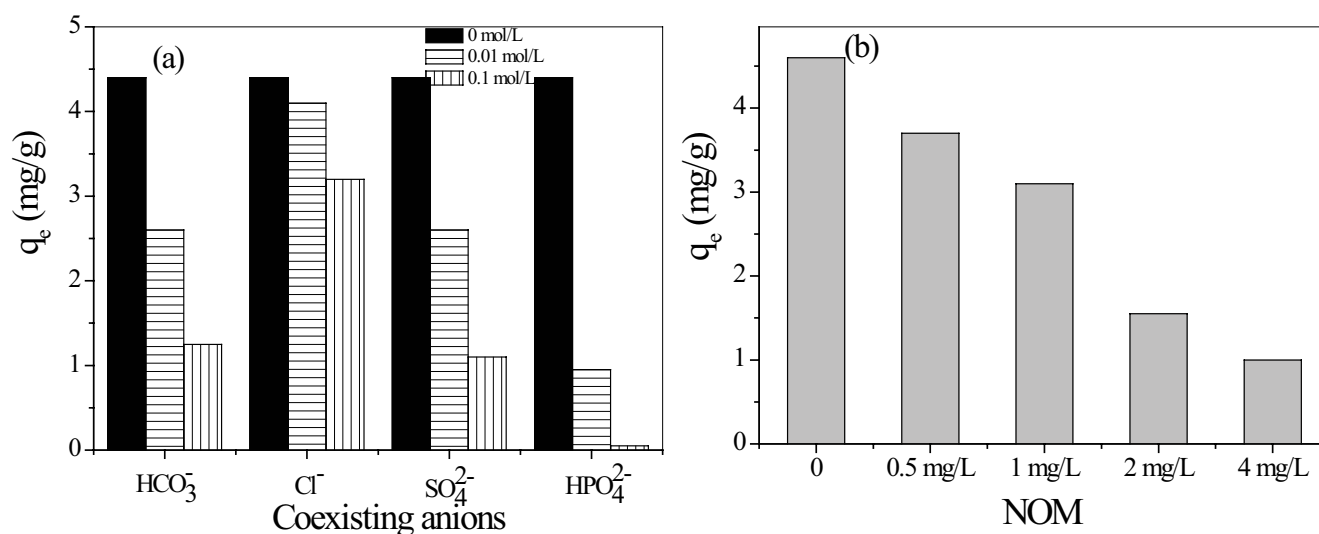


Fig. 7. Effect of coexisting anions (a) and NOM (b) on Mo(VI) uptake.

#### Acknowledgements

The authors are grateful for financial support from the foundation of Henan Water Conservancy Investment Group Corporation (KFJJ201904), Advanced manufacturing of biochar in UK/China/Malaysia/Nigeria (British Council, UK-China-BRI Countries Education Partnership Initiative, 2019), the National Natural Science Foundation of China (Grant no. 51378205) and the Natural Science Foundation of Henan Province (Grant No.182300410136).

#### References

- [1] J.H. Qu, Research progress of novel adsorption processes in water purification: a review, *J. Environ. Sci.*, 20 (2008) 1–13.
- [2] I. Ali, M. Asim, T.A. Khan, Low cost adsorbents for the removal of organic pollutants from wastewater, *J. Environ. Manage.*, 113 (2012) 170–183.
- [3] V.K. Gupta, Suhas, Application of low-cost adsorbents for dye removal – a review, *Environ. Manage.*, 90 (2009) 2313–2342.
- [4] A. Tripathi, M.R. Ranjan, Heavy metal removal from wastewater using low cost adsorbents, *J. Biorem. Biodegrad.*, 6 (2015) 315, doi: 10.4172/2155-6199.1000315.
- [5] J. Lehmann, A handful of carbon, *Nature*, 447 (2007) 143–144.
- [6] M. Ahmad, A.U. Rajapaksha, J.E. Lim, M. Zhang, N. Bolan, D. Mohan, M. Vithanage, S.S. Lee, Y.S. Ok, Biochar as a sorbent for contaminant management in soil and water: a review, *Chemosphere*, 99 (2014) 19–33.
- [7] D. Mohan, A. Sarswat, Y.S. Ok, C.U. Pittman Jr., Organic and inorganic contaminants removal from water with biochar, a renewable, low cost and sustainable adsorbent – a critical review, *Bioresour. Technol.*, 160 (2014) 191–202.
- [8] A.U. Rajapaksha, S.S. Chen, D.C.W. Tsang, M. Zhang, M. Vithanage, S. Mandal, B. Gao, N.S. Bolan, Y.S. Ok, Engineered/designer biochar for contaminant removal/immobilization from soil and water: potential and implication of biochar modification, *Chemosphere*, 148 (2016) 276–291.
- [9] Y.-J. Tu, C.-F. You, C.-K. Chang, T.-S. Chan, S.-H. Li, XANES evidence of molybdenum adsorption onto novel fabricated nano-magnetic  $\text{CuFe}_2\text{O}_4$ , *Chem. Eng. J.*, 244 (2014) 343–349.
- [10] F. Ogata, T. Nakamura, N. Kawasaki, Adsorption capability of virgin and calcined wheat bran for molybdenum present in aqueous solution and elucidating the adsorption mechanism by adsorption isotherms, kinetics, and regeneration, *J. Environ. Chem. Eng.*, 6 (2018) 4459–4466.
- [11] Z.M. Guan, J.F. Lv, P. Bai, X.H. Guo, Boron removal from aqueous solutions by adsorption – a review, *Desalination*, 383 (2016) 29–37.
- [12] R. Brion-Roby, J. Gagnon, S. Nosrati, J.-S. Deschênes, B. Chabot, Adsorption and desorption of molybdenum(VI) in contaminated water using a chitosan sorbent, *J. Water Process Eng.*, 23 (2018) 13–19.
- [13] Y.-C. Chen, C.S. Lu, Kinetics, thermodynamics and regeneration of molybdenum adsorption in aqueous solutions with NaOCl-oxidized multiwalled carbon nanotubes, *J. Ind. Eng. Chem.*, 20 (2014) 2521–2527.
- [14] W.S. Chen, Y.P. Guo, X. Mi, Y. Yu, G.T. Li, Enhanced adsorptive removal of methylene blue by low-temperature biochar derived from municipal activated sludge, *Desal. Water Treat.*, 188 (2020) 257–265.
- [15] M. Abdulkarim, F. Abu Al-Rub, Adsorption of lead ions from aqueous solution onto activated carbon and chemically-modified activated carbon prepared from date pits, *Adsorpt. Sci. Technol.*, 22 (2004) 119–134.
- [16] V. Strelko Jr., D.J. Malik, M. Streat, Characterization of the surface of oxidized carbon adsorbents, *Carbon*, 40 (2002) 95–104.
- [17] Z.W. Zhao, J. Liu, W.T. Xia, C.F. Cao, X.Y. Chen, H.G. Li, Surface complexation modeling of soluble molybdenum adsorption by  $\text{Mn}_2\text{O}_3$ , *J. Chem. Technol. Biotechnol.*, 85 (2010) 121–126.
- [18] F.A. Bertoni, A.C. Medeot, J.C. González, L.F. Sala, S.E. Bellú, Application of green seaweed biomass for Mo(VI) sorption from contaminated waters. Kinetic, thermodynamic and continuous sorption studies, *J. Colloid Interface Sci.*, 446 (2015) 122–132.
- [19] S. Lagergren, Zur theorie der sogenannten adsorption gelöster stoffe, *Kungliga Svenska Vetenskapsakademiens Handlinga*, 24 (1898) 1–39.
- [20] Y.S. Ho, G. McKay, Pseudo-second-order model for sorption process, *Process Biochem.*, 34 (1999) 451–455.
- [21] M. Kithome, J.W. Paul, L.M. Lavkulich, A.A. Bomke, Kinetics of ammonium adsorption and desorption by the natural zeolite clinoptilolite, *Soil Sci. Soc. Am. J.*, 62 (1988) 622–629.
- [22] C.W. Cheung, J.F. Porter, G. McKay, Sorption kinetics for the removal of copper and zinc from effluents using bone char, *Sep. Purif. Technol.*, 19 (2000) 55–64.
- [23] E. Guibal, C. Milot, J.M. Tobin, Metal-anion sorption by chitosan beads: equilibrium and kinetic studies, *Ind. Eng. Chem. Res.*, 37 (1998) 1454–1463.
- [24] N. Yeddou, A. Bensmaili, Kinetic models for the sorption of dye from aqueous solution by clay-wood sawdust mixture, *Desalination*, 185 (2005) 499–508.

- [25] H.M.F. Freundlich, Über die adsorption in lasungen, *J. Phys. Chem.*, 57 (1906) 385–470.
- [26] A. Afkhami, R. Norooz-Asl, Removal, preconcentration and determination of Mo(VI) from water and wastewater samples using maghemite nanoparticles, *Colloids Surf., A*, 346 (2009) 52–57.
- [27] H. Sepehrian, S. Waqif-Husain, J. Fasihi, M.K. Mahani, Adsorption behavior of molybdenum on modified mesoporous zirconium silicates, *Sep. Sci. Technol.*, 45 (2010) 421–426.
- [28] C. Namasivayam, D. Sangeetha, Removal of molybdate from water by adsorption onto ZnCl<sub>2</sub> activated coir pith carbon, *Bioresour. Technol.*, 97 (2006) 1194–1200.
- [29] C. Namasivayam, K. Prathap, Uptake of molybdate by adsorption onto industrial solid waste Fe(III)/Cr(III) hydroxide: kinetic and equilibrium studies, *Environ. Technol.*, 27 (2006) 923–932.
- [30] G. Dodbiba, T. Fujita, T. Kikuchi, J. Manjanna, S. Matsuo, H. Takahashi, K. Tohji, Synthesis of iron-based adsorbents and their application in the adsorption of molybdenum ions in nitric acid solution, *Chem. Eng. J.*, 166 (2011) 496–503.
- [31] N. Fallah, M. Taghizadeh, S. Hassanpour, Selective adsorption of Mo(VI) ions from aqueous solution using a surface-grafted Mo(VI) ion imprinted polymer, *Polymer*, 144 (2018) 80–91.
- [32] X. Wang, Y. Zhang, Q.M. Li, Characterization and determination of the thermodynamic and kinetic properties of the adsorption of molybdenum(VI) onto microcrystalline anthracene modified with 8-hydroxyquinoline, *Mater. Sci. Eng. C*, 31 (2011) 1826–1831.
- [33] X. Yuan, W. Xing, S.-P. Zhuo, Z.H. Han, G.Q. Wang, X.L. Gao, Z.-F. Yan, Preparation and application of mesoporous Fe/carbon composites as a drug carrier, *Microporous Mesoporous Mater.*, 117 (2009) 678–684.
- [34] S. Altenor, B. Carene, E. Emmanuel, J. Lambert, J.-J. Ehrhardt, S. Gaspard, Adsorption studies of methylene blue and phenol onto vetiver roots activated carbon prepared by chemical activation, *J. Hazard. Mater.*, 165 (2009) 1029–1039.
- [35] M. Pumera, B. Šmíd, K. Veltruská, Influence of nitric acid treatment of carbon nanotubes on their physico-chemical properties, *J. Nanosci. Nanotechnol.*, 9 (2009) 2671–2676.
- [36] C.S. Lu, C.T. Liu, F.S. Su, Sorption kinetics, thermodynamics and competition of Ni<sup>2+</sup> from aqueous solutions onto surface oxidized carbon nanotubes, *Desalination*, 249 (2009) 18–23.